ANS RPSD 2018 - 20th Topical Meeting of the Radiation Protection & Shielding Division of ANS
Santa Fe, NM, August 26 – 31, 2018, on CD-ROM, American Nuclear Society, LaGrange Park, IL (2018)

SAND2018-8103C

SPECIALIZATIONS IN THE SCEPTRE CODE FOR CHARGED-PARTICLE TRANSPORT

Clif Drumm[1], Wesley Fan[1], and Shawn Pautz[1]

[1]*Sandia National Laboratories, Radiation Effects Theory Dept. PO Box 5800, Albuquerque, NM 87111*
crdrumm@sandia.gov
wcfan@sandia.gov
sdpautz@sandia.gov

Charged particles present some unique challenges for radiation transport codes. This is because charged particles have cross sections that are extremely forward peaked, are huge in the limit of small energy transfer, and are highly scattering, which causes slow convergence of the source iterations. The primary application of SCEPTRE is modeling radiation-driven electrical effects, so substantial effort has been invested in SCEPTRE for the efficient modeling of electron transport. This paper will summarize recent and ongoing activities involving the accurate deterministic-transport modeling of charged particles and methods implemented to improve iterative convergence.

I. INTRODUCTION

The SCEPTRE[1] (Sandia Computational Engine for Particle Transport for Radiation Effects) radiation transport code has several mature and ongoing development efforts supporting the accurate and efficient modeling of electron transport[2-5]. Although SCEPTRE is a general-purpose radiation transport code, which may be used for any particle type for which cross-section information is provided, the primary application of SCEPTRE is modeling radiation-driven electrical effects. For this reason, substantial effort has been invested in SCEPTRE since its inception for the efficient modeling of electron/positron transport. SCEPTRE has also been applied to proton transport analyses.

Charged particles present some unique challenges for radiation transport codes, because charged particles have cross sections that are extremely forward peaked, are huge in the limit of small energy transfer, and are highly scattering, which causes slow convergence of the source iterations. This work summarizes mature capabilities that have been productized in SCEPTRE as well as some ongoing development efforts for the efficient and accurate modeling of charged-particle transport.

The paper presents brief summaries of four topics:

1. A comparison of the Galerkin-quadrature[6] approach and the δ-function down scattering approach[2] to accurately model the extreme forward peakedness of electron scattering.
2. The application of Transport Synthetic Acceleration (TSA) for improving convergence of the scattering-source iterations for highly-scattering media[3].
3. The application of Discontinuous-Galerkin Finite Elements (DGFE) in energy as an alternative to a multigroup treatment of the energy dependence of the particle transport[4].
4. Modeling charged-particle transport in the presence of externally-imposed ElectroMagnetic (EM) fields[5].

The first two topics have been productized into SCEPTRE and are at a mature development stage, while the last two topics are more experimental and are under ongoing development. Results obtained from SCEPTRE computations will be compared with experimental data, where available, Monte Carlo results, and Method of Manufactured Solutions (MMS) results.

II. GALERKIN QUADRATURE VS. EXPLICIT δ-FUNCTION DOWNSCATTER

Because of the extreme forward peaked nature of charged-particle scattering a standard MultiGroup-Legendre (MGL) treatment is impractical. SCEPTRE includes two methods for accurately modeling the extreme anisotropy in the scattering: 1) explicit modeling of a δ-function down-scatter term[2], and 2) using a Galerkin quadrature/moments method[6].

Both methods are based on the Boltzmann-CSD equation,

$$\begin{aligned}\boldsymbol{\Omega}\cdot\nabla\psi+\sigma_t\psi(\boldsymbol{r},\boldsymbol{\Omega},E)-\frac{\partial(S_R\psi)}{\partial E}\\ =\int_{E+\Delta}^{E_{max}}\int_{4\pi}\sigma_s(\mu_0,E'\to E)\psi(\boldsymbol{r},\boldsymbol{\Omega}',E')d\boldsymbol{\Omega}'dE'\\ +Q(\boldsymbol{r},\boldsymbol{\Omega},E),\end{aligned} \tag{1}$$

subject to appropriate boundary conditions at the physical boundaries and at the upper-energy boundary. $Q(\boldsymbol{r},\boldsymbol{\Omega},E)$ is an external fixed source, and $S_R(E)$ is a restricted stopping power, which includes the most forward-peaked component of the inelastic scattering,

$$S_R(E)=\int_{E-\Delta}^{E}(E-E')\sigma_s(E\longrightarrow E')dE', \tag{2}$$

where Δ is an arbitrarily-chosen energy transfer marking the division between the CSD and MGL treatments of the scattering.

For both methods, cross sections are obtained from the CEPXS[7] code. For the explicit modeling of a δ-function down-scatter component, the scattering cross sections are approximated by

$$\sigma_{g'\to g}(\mu_0) \cong \sum_{l=0}^{L} \tilde{\sigma}^{l}_{g'\to g}\, P_l(\mu_0) + \sigma^{L+1}_{g'\to g}\delta(1-\mu_0), \tag{3}$$

where modified scattering moments are defined as

$$\tilde{\sigma}^{l}_{g'\to g} \equiv \sigma^{l}_{g'\to g} - \sigma^{L+1}_{g'\to g}. \tag{4}$$

The multigroup-Legendre transport equation can be written as,

$$\boldsymbol{\Omega}\cdot\nabla\psi_g + \sigma_{t,g}\psi_g = \left\{\sum_{g'}[M]\left[\tilde{\Sigma}_{g'\to g}\right][D] + \Sigma^{L+1}_{g'\to g}\right\}\psi_{g'} + Q_g, \tag{5}$$

where $[D]$ and $[M]$ are discrete-to-moment and moment-to-discrete matrices, respectively, which are obtained from the specific angular quadrature and angular moments used in the calculation. $\left[\tilde{\Sigma}_{g'\to g}\right]$ is a diagonal matrix containing the modified scattering moments.

For the Galerkin quadrature/moments method, a requirement is placed on $[D]$ such that the discrete-to-moment matrix is the inverse of the moment-to-discrete matrix,

$$[D] = [M]^{-1}. \tag{6}$$

This requires that the matrices be square, e.g. the number of discrete directions is equal to the number of angular moments. Furthermore, $[M]$ must be invertible.

Morel[6] provides a prescription for an appropriate set of angular moments such that Eq. (6) is satisfied for Gauss-Legendre quadrature in one-dimensional geometry and level-symmetric quadrature in multi-dimensional geometries. SCEPTRE also includes Gauss-Lobatto quadrature in one-dimensional geometry and Lebedev quadrature for multi-dimensional geometries, and for these quadratures, a Gram-Schmidt orthogonalization procedure developed by J. Chenhall is used to determine appropriate set of angular moments[8].

The scattering term includes a similarity transformation of the scattering-moments matrix,

$$\boldsymbol{\Omega}\cdot\nabla\psi_g + \sigma_{t,g}\psi_g = \sum_{g'}[M]\left[\Sigma_{g'\to g}\right][M]^{-1}\psi_{g'} + Q_g. \tag{7}$$

As is evident from Eq. (7), this method also exactly integrates a δ-function component of the scattering, so the two methods are very similar.

The two methods are compared by computing the energy-deposition distributions for electrons incident upon various materials, as measured by Lockwood, et al.[9]. The calculations use a Gauss-Lobotto angular quadrature and very fine spatial mesh. Both low- and high-order angular quadrature were used in the comparisons. Results for Be, Al, and U are shown in Figs. 1a-1c, for electrons incident from the left.

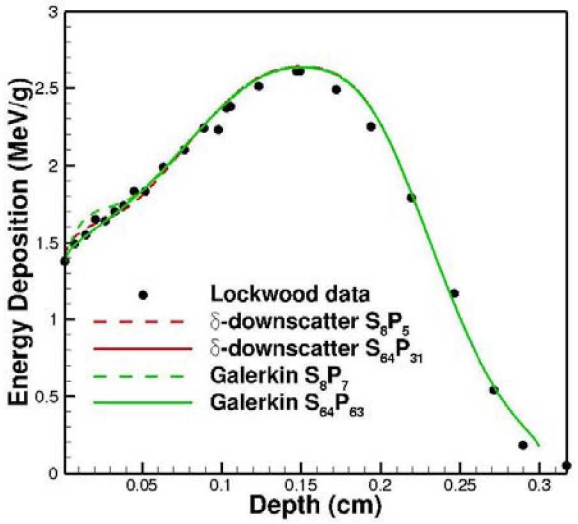

Fig. 1a. 1.033-MeV electrons on beryllium energy deposition.

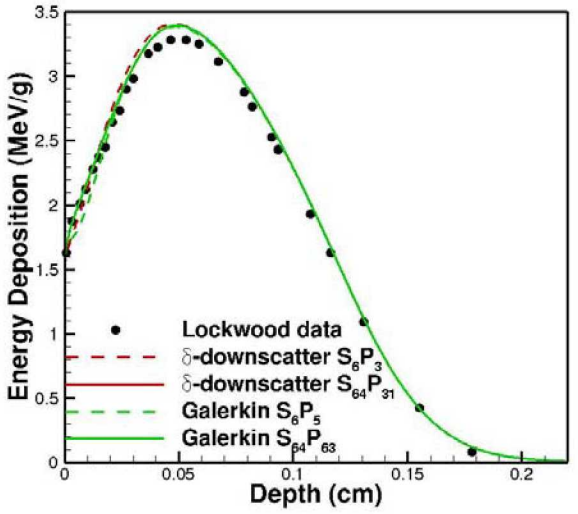

Fig. 1b. 1.033-MeV electrons on aluminum energy deposition.

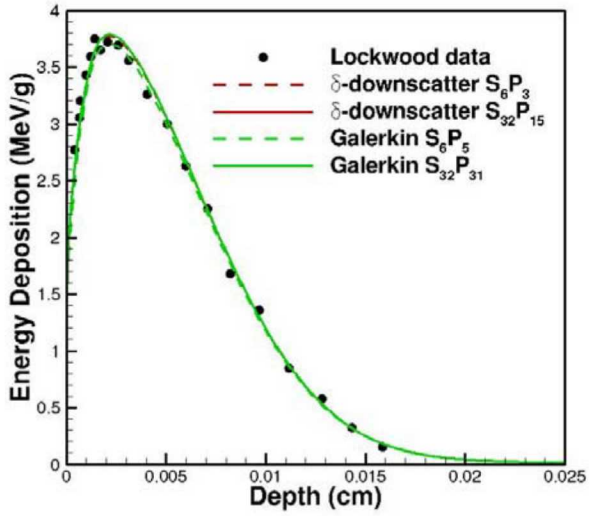

Fig. 1c. 1.0-MeV electrons on uranium energy deposition.

For the high-order angular quadratures, the results from both methods are indistinguishable from each other and compare well with the measured data. For the low-order angular quadratures, both methods agree well except for near the incident surface, where slight oscillations are evident for Be and Al, with the δ-function downscatter performing perhaps slightly better. For U neither method shows oscillations even for the low-order angular quadrature.

For the Galerkin method, the angular moments set is not independent, but chosen to generate a square, invertible moment-to-discrete matrix. For one-dimensional geometries, this requires that the order of the angular moments set be one less than the order of the angular quadrature, and for multi-dimensional geometries a few additional higher-order moments need to be included.

For the δ-downscatter method, the angular quadrature and angular moments can be specified independently. However, the order of the angular quadrature must be high enough to accurately integrate the angular moments. Runtimes for the two methods are comparable for the same quadrature order.

II. ACCELERATION OF THE SCATTERING SOURCE ITERATIONS

Convergence of unaccelerated scattering-source iterations is slow for highly-scattering charged particles, necessitating some type of acceleration to make transport calculations practical. In addition to a sweeps-based source-iteration solver, SCEPTRE contains several alternative solvers using a simultaneous space-angle solve using a Krylov solver from the Trilinos package[10].These solvers have entirely different convergence properties than source iteration[3], making them useful as coarse-level solvers in a TSA method.

Based on these Krylov solvers, SCEPTRE has a flexible TSA algorithm that uses a low-order discrete-ordinates (S_N) or spherical-harmonics (P_N) solve to accelerate convergence of a high-order S_N Source-Iteration (SI) solve. Convergence of the low-order solves can be further accelerated by applying off-the-shelf Incomplete-Factorization (IF) or Algebraic-MultiGrid (AMG) methods, included in the Trilinos packages[10]. Convergence of the Krylov methods depends upon the condition number of the system matrix and the clustering of the eigenvalues, rather than upon the scattering ratio, so that rapid convergence may be obtained even when highly-scattering media is present in the problem. Practical transport problems often include both highly-scattering regions and streaming regions, making preconditioner effectiveness highly problem dependent, but speed-up factors around ten have been typically observed in applications.

The TSA algorithms have many options available for controlling both the coarse-level solves and the coarse-level acceleration. One of the key factors affecting overall runtime is the specified convergence tolerance and/or maximum number of iterations for the coarse level solves. Often, running a small number of coarse-level iterations, resulting in a crude approximation to the correction term, may result in a good speed up in the convergence of the fine-level source iterations.

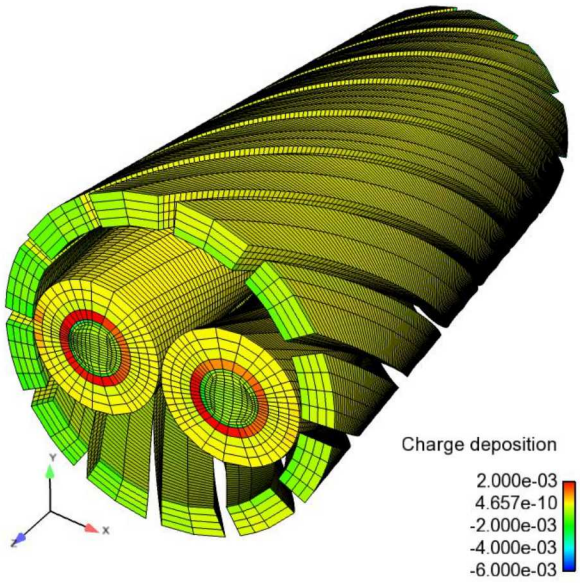

Fig. 2a. Charge-deposition distribution in braided-shield twisted-pair cable segment.

As a test of the TSA methods, we modeled a segment of a braided-shield twisted-pair cable with copper conductors, shown in Figs. 2a and 2b. A planar source of 50-keV photons was incident approximately along the positive x-axis. The spatial mesh contained about a half-million linear hexahedral (hex8) elements, and the angular approximation used S_8 level-symmetric quadrature with P_3

scattering, including a δ-function down scatter term. 10 linear-photon and 10 log-electron energy groups were used, and cross sections were obtained from CEPXS[7].

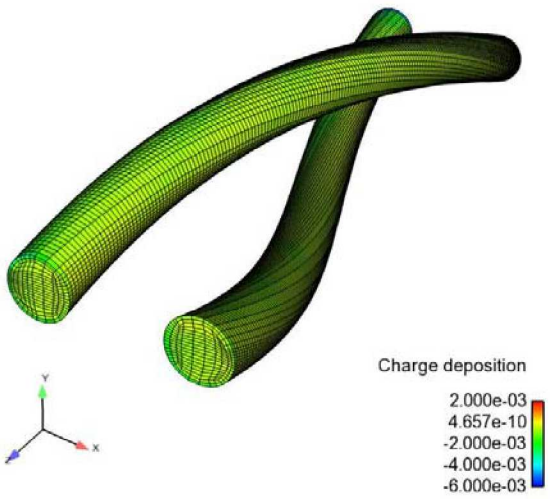

Fig. 2b. Twisted-pair cable segment with shield removed to reveal the conductor pairs.

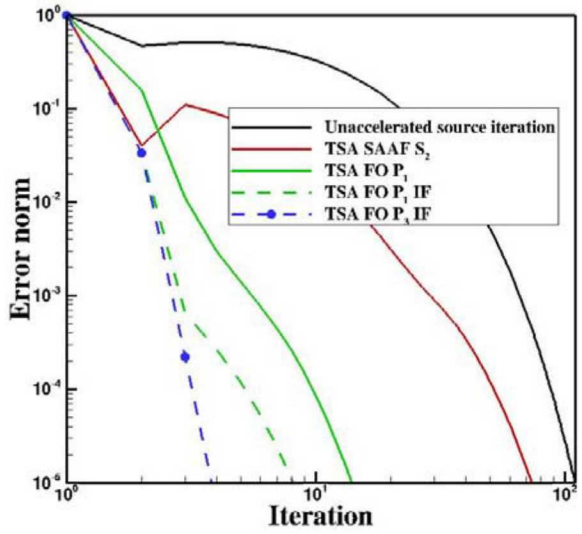

Fig. 3a. Convergence of the 5th electron group iterations for various TSA solvers

Fig. 3a compares the iteration convergence for the 5th electron group for various TSA methods compared with unaccelerated SI. TSA methods compared include: S_N Self-Adjoint Angular Flux (SAAF)[11], and P_N First-Order (FO), with and without IF acceleration of the coarse-level solves. The scattering ratio for this electron group is 0.905 in copper.

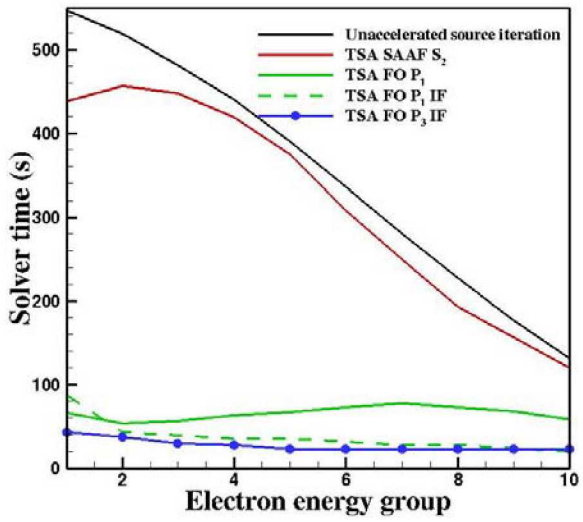

Fig. 3b. Solve times for the electron groups for various TSA solvers.

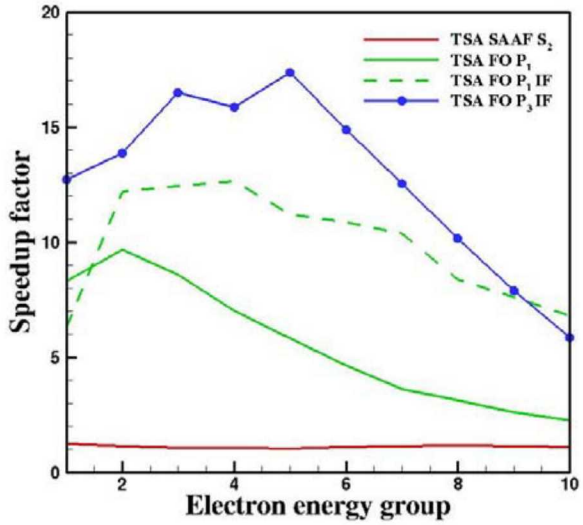

Fig. 3c. Speedup factors relative to unaccelerated sweeps for electron groups for various TSA solvers

Solve time versus electron energy group is shown in Fig. 3b for the various acceleration methods, and speed-up factors are shown in Fig. 3c. For this test problem, FO P_3 TSA with IF performed the best, in terms of both convergence rate and solve time. SAAF performed poorly for this test problem, being only slightly faster than unaccelerated SI. The reason for this is that the transport problem is based on Discontinous Finite Elements (DFE), while the SAAF coarse-level solver is based on Continuous Finite Elements (CFE), which degrades the effectiveness of SAAF as a coarse-level solver. The advantage of the SAAF method is that it results in a Symmetric Positive

Definite (SPD) linear system that is solved using a highly-efficient Conjugate Gradients (CG) algorithm, while the FO solvers use a less-efficient GMRES algorithm. The use of a CG solver results in much fast coarse-level solves, but, for this test problem, the greater effectiveness of the DFE FO solve as an accelerator more than offsets the efficiency of CG.

The timings were obtained by running on a TLCC2 machine, using 256 Intel Sandy Bridge 2.6 GHz cores. The convergence tolerance for the fine-level sweeps was an L2 error norm of 10^{-5}.

Parameters for the coarse-level solves and overall runtimes and speedup factors are shown in Table I.

TABLE I. TSA convergence metrics and total solve time for electron groups for various acceleration methods.

TSA method	Coarse-level parameters			Total solve time of electron groups (s)	Speed up
	Preconditioner	Convergence tolerance	Max iterations		
none	-	-	-	3530	1
FO P_1	none	0.01	100	653	5.4
FO P_1	IF	0.01	10	365	9.7
FO P_3	IF	0.01	10	272	13.
SAAF S_2	none	10^{-4}	1000	3160	1.1

III. FINITE-ELEMENTS IN ENERGY

SCEPTRE includes experimental capability for using finite elements in energy as an alternative to multigroup. Starting with the Boltzmann-CSD equation, Eq. (1), the angular flux and source terms are expanded in linear or quadratic energy basis functions, $\varphi_g^{i'}(E)$ which are defined over an energy group (element),

$$\psi(\boldsymbol{r},\boldsymbol{\Omega},E) \cong \tilde{\psi}(\boldsymbol{r},\boldsymbol{\Omega},E) = \sum_{i'} \psi_g^{i'}(\boldsymbol{r},\boldsymbol{\Omega})\varphi_g^{i'}(E), \quad (8a)$$

and

$$Q(\boldsymbol{r},\boldsymbol{\Omega},E) \cong \tilde{Q}(\boldsymbol{r},\boldsymbol{\Omega},E) = \sum_{i'} q_g^{i'}(\boldsymbol{r},\boldsymbol{\Omega})\varphi_g^{i'}(E), \quad (8b)$$

where $\psi_g^{i'}(\boldsymbol{r},\boldsymbol{\Omega})$ and $q_g^{i'}(\boldsymbol{r},\boldsymbol{\Omega})$ are the expansion coefficient for the angular flux and source terms, respectively, for energy group g and energy basis i'. The source term includes both the external fixed source and the scattering source.

Applying DGFE to the energy variable, the Boltzmann-CSD equation becomes[4, 12]

$$\begin{aligned}&\sum_{i'}\Big[\boldsymbol{\Omega}\cdot\nabla\psi_g^{i'}\langle\varphi_g^i(E),\varphi_g^{i'}(E)\rangle + \\ &\psi_g^{i'}(\boldsymbol{r},\boldsymbol{\Omega})\langle\varphi_g^i(E),\sigma_t(E)\varphi_g^{i'}(E)\rangle + \\ &\psi_g^{i'}(\boldsymbol{r},\boldsymbol{\Omega})\langle\tfrac{d\varphi_g^i}{dE},S_R(E)\varphi_g^{i'}\rangle\Big] + \\ &S_R(E_{g,l})\psi_g^{i_l}(\boldsymbol{r},\boldsymbol{\Omega}) = S_R(E_{g-1,l})\psi_{g-1}^{i_l}(\boldsymbol{r},\boldsymbol{\Omega}) + \\ &\sum_{i'}\left[q_g^{i'}(\boldsymbol{r},\boldsymbol{\Omega})\langle\varphi_g^i(E),\varphi_g^{i'}(E)\rangle\right]\end{aligned} \quad (9)$$

$\langle\varphi_g^i(E),\varphi_g^{i'}(E)\rangle$ are the elements of the energy mass matrix, $\langle\varphi_g^i(E),\sigma_t(E)\varphi_g^{i'}(E)\rangle$ are the elements of the weighted total cross section matrix, $\langle\frac{d\varphi_g^i}{dE},S_R(E)\varphi_g^{i'}\rangle$ are the elements of the weighted restricted stopping power matrix, and $S_R(E_{g,l})$ and $S_R(E_{g-1,l})$ are the stopping power values at the energy element boundaries.

We currently do not have the capability of computing energy FE weighted cross sections and stopping powers, so we use standard MGL cross sections and stopping powers computed by CEPXS[7] until this capability is developed. This introduces some additional error in the results.

Fig. 5 shows the electron emission spectrum for 1-MeV electrons normally incident on approximately 0.6-range-thick aluminum. The figure compares results from SCEPTRE using DGFE in energy with ITS Monte Carlo[13] and measured data[14]. The description of the experiment indicates that the aluminum thickness was 0.32 g/cm^3 or about 0.6-range-thick. Using 0.555 g/cm^2 as the CSDA

range and aluminum density of 2.7 g/cm^3 indicates about a 4% uncertainty in the aluminum thickness, which has a major impact on the calculated electron emission spectra. The transport calculations were performed with two different aluminum thicknesses, 0.1232 cm and 0.1185 cm, spanning the uncertainty in the reported thickness.

The results agree reasonably well. The SCEPTRE results are about 5% higher than the Monte Carlo results at the peak. The reason for this difference is not known at the present time. Using 0.1185-cm-thick aluminum, the calculated magnitude of the peak matches the experimental results well, but the spectral shape is shifted toward higher energy. Using 0.1232-cm-thick aluminum, the calculated spectral shapes agree well with the measured values, but the calculated magnitude of the peak is about 20% lower than the measured value.

For this problem, run times for SCEPTRE and ITS were comparable. However, since the runs were very fast, neither calculation was optimized for speed. The SCEPTRE run time was 35 s for 100 spatial elements, 200 energy elements, S_{16} Gauss-Lobatto angular quadrature, P_7 scattering, with an iterative convergence tolerance of 10^{-12}. The ITS run time was 119 s for 10^7 histories, which was sufficient to reduce the relative standard error to <2% for each of 200 energy bins with values >5% of the maximum electron emission. The SCEPTRE run was on performed in serial on a 3.1 GHz XEON processor, and the ITS run was performed in parallel on 12 3.1 GHz XEON processors.

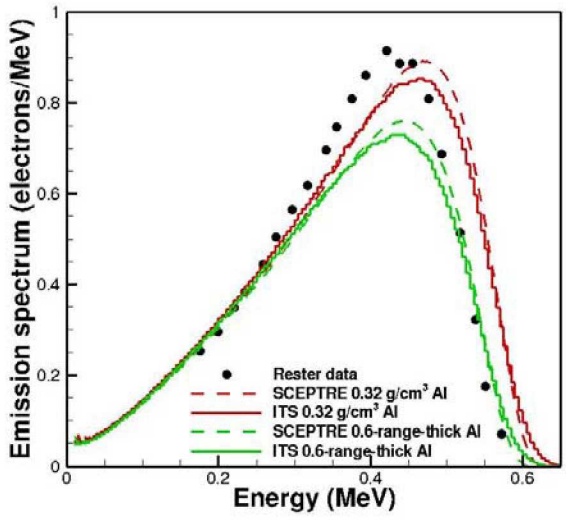

Fig. 5. Electron emission from 1-MeV electrons on 0.6-range aluminum.

IV. TRANSPORT WITH ELECTROMAGNETIC FIELDS PRESENT

The inclusion of EM fields greatly complicates the transport equation. Eq. (10) shows the Boltzmann-Vlasov for transport of relativistic charged particles in the presence of EM fields.

$$\begin{aligned}&\frac{1}{v}\frac{\partial\psi}{\partial t}+\boldsymbol{\Omega}\cdot\nabla\psi+\sigma\psi+q(\boldsymbol{\mathcal{E}}\cdot\boldsymbol{\Omega})\left[\frac{\partial\psi}{\partial E}-\frac{1+4\beta^2}{\mathcal{D}(E)}\psi\right]+\frac{q}{\mathcal{D}(E)}\left[\mathcal{E}_x(1-\mu^2)-\mathcal{E}_y\mu\eta-\mathcal{E}_z\mu\xi+v\left(\mathcal{B}_z\eta-\mathcal{B}_y\xi\right)\right]\frac{\partial\psi}{\partial\mu}+\\&\frac{q}{\mathcal{D}(E)(1-\mu^2)}\left[\mathcal{E}_z\eta-\mathcal{E}_y\xi+v\left[\mathcal{B}_y\mu\eta+\mathcal{B}_z\mu\xi-\mathcal{B}_x(1-\mu^2)\right]\right]\frac{\partial\psi}{\partial\varphi}=Q,\end{aligned}\tag{10}$$

where $\boldsymbol{\mathcal{D}(E)}$ is given by,

$$\mathcal{D}(E)=\frac{E\left(E+2m_0c^2\right)}{E+2m_0c^2}.\tag{11}$$

The electric and magnetic field vectors are given by,

$$\begin{aligned}\boldsymbol{\mathcal{E}}&=\mathcal{E}_x\boldsymbol{i}+\mathcal{E}_y\boldsymbol{j}+\mathcal{E}_z\boldsymbol{k}\\\boldsymbol{\mathcal{B}}&=\mathcal{B}_x\boldsymbol{i}+\mathcal{B}_y\boldsymbol{j}+\mathcal{B}_z\boldsymbol{k}.\end{aligned}\tag{12}$$

SCEPTRE contains experimental capability for solving the Boltzmann-Vlasov equation, using finite elements in space, angle and energy[5].

Results for two simple test problems are shown here. The first is an MMS test problem in one-dimensional geometry, in a void region with a uniform electric field present. The MMS angular flux is chosen to be

$$\psi(x,\mu,E)=\sqrt{E}(\mu^2E-x),\tag{13}$$

which is shown in Fig. 6a for $\boldsymbol{x=0.5}$.

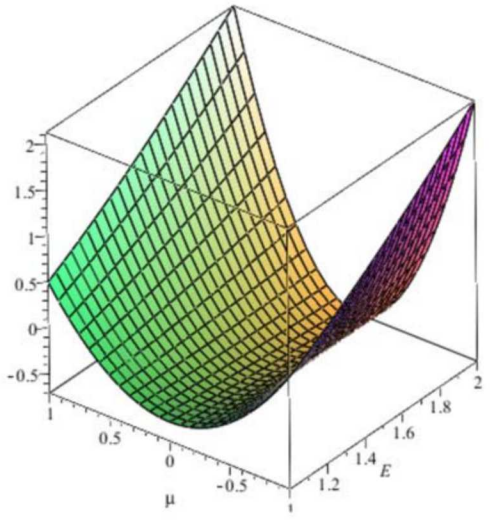

Fig. 6a. Analytic solution for transport in vacuum.

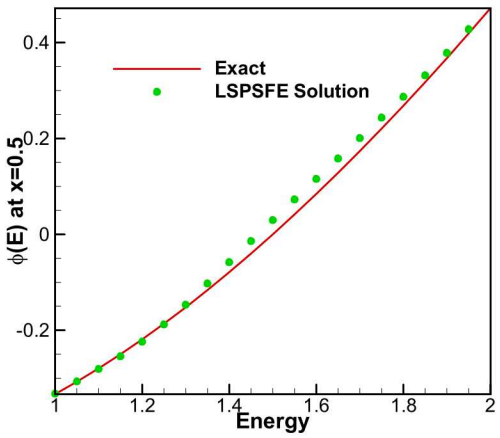

Fig. 6b. LSPSFE energy dependence of scalar flux compared with exact solution

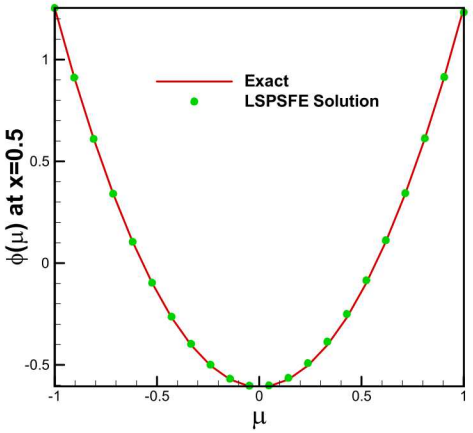

Fig. 6c. LSPSFE angular flux compared with exact solution

The energy and angle dependence of the SCEPTRE Least-Squares Phase-Space Finite-Elements (LSPSFE) solutions are compared with the analytic solution in Figs. 6b and 6c.

A second test problem consists of a plane wave of electrons with a grazing incidence in the +y direction on the bottom of a three-dimensional void region, in which a uniform magnetic field is applied in the +x direction. Physically the electrons should travel in a circle in the y-z plane, initially moving in the +y direction, then successively the +z, -y, and –z directions before exiting the bottom surface. A slice of the calculated solution (with approximately 20 elements in each of the spatial and angular dimensions) is shown in Fig. 7. These results show the correct sinusoidal variation in angle and space with no change in particle energy.

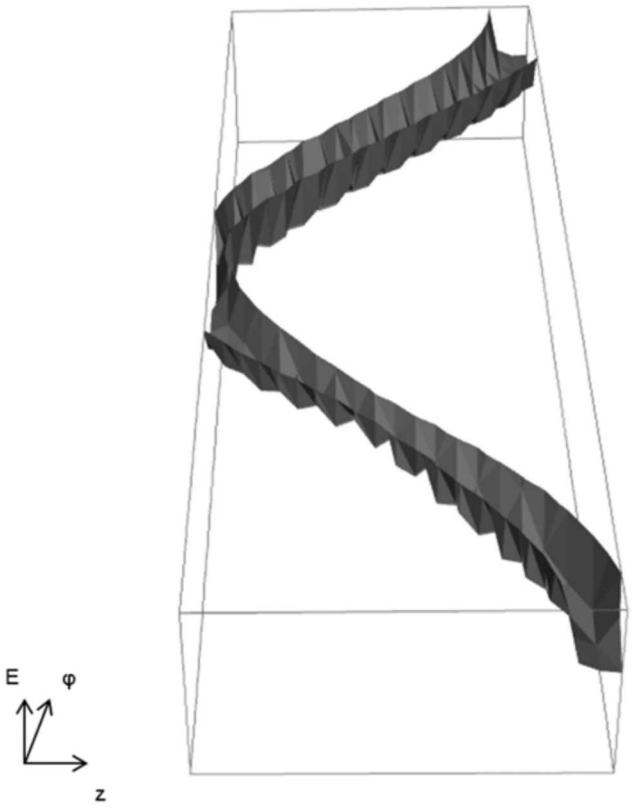

Fig. 7. Electron transport in void with constant magnetic field (slice through phase-space).

V. CONCLUSIONS

Capabilities for the accurate and efficient modeling of electron transport with SCEPTRE have been presented. As the complete phase-space finite elements capability is productized, SCEPTRE will be able to handle more challenging transport problems, including transport in the presence of externally applied electric and magnetic fields. Fully utilizing the capabilities requires computation of finite-element weighted cross sections and stopping powers, which is currently under active development.

ACKNOWLEDGMENTS

Sandia National Laboratories is a multimission laboratory managed and operated by National Technology and Engineering Solutions of Sandia, LLC, a wholly owned subsidiary of Honeywell International, Inc., for the U.S. Department of Energy's National Nuclear Security Administration under contract DE-NA000352.

This paper describes objective technical results and analysis. Any subjective views or opinions that might be expressed in the paper do not necessarily represent the views of the U.S. Department of Energy or the United States Government.

REFERENCES

1. S. PAUTZ, W. BOHNHOFF, C. DRUMM and W. FAN, "Parallel Discrete Ordinates Methods in the SCEPTRE Project," *Proc. M&C 2009,* Saratoga Springs, New York, May 3-7, 2009, American Nuclear Society (2009).
2. C. DRUMM, W. FAN, L. LORENCE, and J. POWELL, "An Analysis of the Extended-Transport Correction with Application to Electron Beam Transport," *Nucl. Sci. Eng.,* **155**, 355 (2007).
3. C. DRUMM and W. FAN, "Multi-Level Acceleration of Scattering-Source Iterations with Application to Electron Transport," *Nucl. Eng. Tech.,* **49**, 1114 (2017).
4. C. DRUMM, W. FAN, and S. PAUTZ, "Phase-Space Finite Elements in a Least-Squares Solution of the Transport Equation," *Proc. M&C 2013,* Sun Valley, Idaho, May 5-9, 2013, American Nuclear Society (2013).
5. S. PAUTZ, C. DRUMM, W FAN AND C D TURNER, "A Discontinuous Phase-Space Finite Element Discretization of the Linear Boltzmann-Vlasov Equation for Charged Particle Transport," *J. Comp. and Theor. Transport,* **43**, 128 (2014).
6. J. MOREL, "A Hybrid Collocation-Galerkin-Sn Method for Solving the Boltzmann Transport Equation," *Nucl. Sci. Eng.,* **101**, 72 (1989).
7. L. LORENCE, J. MOREL, and G. VALDEZ, "Physics Guide to CEPXS: A Multigroup Coupled Electron-Photon Cross-Section Generating Code Version 1.0," Sandia National Laboratories report, SAND79-0414, Albuquerque, NM (reprinted 1987).
8. C. DRUMM, W. FAN, A. BIELEN and J. CHENHALL, "Least Squares Finite Elements Algorithms in the SCEPTRE Radiation Transport Code," *Proc. M&C 2011*, Rio de Janeiro, Brazil, May 8-12, 2011, American Nuclear Socity (2011).
9. G. LOCKWOOD, L. RUGGLES, G. MILLER and J. HALBLEIB, "Calorimetric Measurement of Electron Energy Deposition in Extended Media- Theory vs Experiment," Sandia National Laboratories report, SAND79-0414, Albuquerque, NM (reprinted 1987).
10. M. HEROUX, et. al, "An Overview of Trilinos", Sandia National Laboratories report, SAND2003-2927, Albuquerque, NM (2003).
11. J. MOREL and J. MCGHEE, "A Self-Adjoint Angular Flux Equation," *Nucl. Sci. Eng.,* **132**, 312 (1999).
12. C. DRUMM and R. KENSEK, "Scattering Cross Sections for Electron Transport Using Energy-Finite-Element Weighting," *Proc. M&C 2017*, Jeju, Korea, April 16-20, 2017, American Nuclear Society (2017).
13. B. FRANKE, R. KENSEK, and T. LAUB, "ITS Version 5.0: The Integrated TIGER Series of Coupled Electron/Photon Monte Carlo Transport Codes with CAD Geometry," Sandia National Laboratories report, SAND2004-5172, Albuquerque, NM (2005).
14. D. RESTER and J. DERRICKSON, "Electron Transmission Measurements for Al, Sn, and Au Targets at Electron Bombarding Energies of 1.0 and 2.5 MeV," *J. App. Phys.*, **42**, 714 (1971).